

A COMPARISON OF THE RADIO AND OPTICAL TIME-EVOLUTION OF HH 1 AND 2

L. F. Rodríguez¹, A. C. Raga², A. Rodríguez-Kamenetzky^{1,3}, and C. Carrasco-González¹

Received June 26 2017; accepted September 14 2017

ABSTRACT

We present a comparison between the time-evolution over the past ≈ 20 years of the radio continuum and H α emission of HH 1 and 2. We find that the radio continuum and the H α emission of both objects show very similar trends, with HH 1 becoming fainter and HH 2 brightening quite considerably (by about a factor of 2). We also find that the $F_{\text{H}\alpha}/F_{\text{ff}}$ (H α to free-free continuum) ratio of HH 1 and 2 has higher values than the ones typically found in planetary nebulae (PNe), which we interpret as an indication that the H α and free-free emission of HH 1/2 is produced in emitting regions with lower temperatures (≈ 2000 K) than the emission of PNe (with $\approx 10^4$ K).

RESUMEN

Presentamos una comparación entre la evolución temporal en los pasados ≈ 20 años de la emisión de radio continuo y de H α de HH 1 y 2. Encontramos que el radio continuo y H α de los dos objetos muestran evoluciones similares, con HH 1 debilitándose y HH 2 volviéndose considerablemente más brillante (aproximadamente un factor de 2). También encontramos que el cociente $F_{\text{H}\alpha}/F_{\text{ff}}$ (entre H α y el radio continuo) de HH 1 y 2 tiene valores mayores que los encontrados típicamente en nebulosas planetarias (PNe), lo cual interpretamos como una indicación de que la emisión libre-libre y de H α de HH 1/2 se produce en regiones con temperaturas menores (≈ 2000 K) que la emisión de las PNe (con $\approx 10^4$ K).

Key Words: Herbig-Haro objects — ISM: individual objects: HH1/2 — ISM: jets and outflows — ISM: kinematics and dynamics — shock waves — stars: winds, outflows

1. INTRODUCTION

HH 1 and 2 were the first discovered Herbig-Haro (HH) objects (Herbig 1951; Haro 1952). Their diverging proper motions (Herbig & Jones 1981) show that they correspond to the two lobes of a bipolar outflow. This outflow was first thought to be ejected by the Cohen-Schwartz (C-S) star, located closer to HH 1 (Cohen & Schwartz 1979), but was later shown to be ejected from the VLA 1 radio source (Pravdo et al. 1985), centrally located between HH 1 and 2.

The radio continuum emission of HH 1 and 2 is clearly detected in maps obtained with the Very

Large Array (VLA) interferometer (Pravdo et al. 1985). The radio emission of these objects shares the proper motions of their optical counterparts (Rodríguez et al. 1990).

The optical emission of HH 1 and 2 also shows relatively strong time variabilities (Herbig 1968, 1973). Raga et al. (2016a) used Hubble Space Telescope (HST) narrow-band images to show that during the last ≈ 20 years HH 1 has become fainter and HH 2 has brightened quite considerably. In the present paper we show that the radio continuum emission of these objects shows similar trends.

To this effect, we have generated a 4.86 GHz map using archival VLA observations with a number of epochs centered around 1988, and a new map ob-

¹Instituto de Radioastronomía y Astrofísica, UNAM, México.

²Instituto de Ciencias Nucleares, UNAM, México.

³Instituto de Astronomía Teórica y Experimental, (IATE-UNC), Argentina.

tained with the Karl G. Jansky Very Large Array in 2012. These maps (as well as the HST H α images) are described in § 2.

We carry out a comparison of the radio continuum and H α morphologies in § 3, and calculate the angularly integrated emission in § 4. A comparison between the radio continuum to H α ratios of HH 1 and 2 with the ones obtained for planetary nebulae is made in § 5. Finally, the results are summarized in § 6.

2. THE OBSERVATIONS

2.1. Very Large Array

The first image of the HH 1/2 region was made with the Very Large Array (VLA) of NRAO⁴ at C-band (4.86 GHz) using data from 11 epochs between 1984 October 02 and 1992 December 19. The parameters of these observations are listed in Table 1 of Rodríguez et al. (2016). The average epoch of these data is 1988.01. These observations were all made with the phase center at or very close to the position of HH 1/2 VLA 1 [$\alpha(J2000) = 05^h 36^m 22^s.84$; $\delta(J2000) = -06^\circ 46' 06''.2$], the exciting source of the HH 1/2 system (Pravdo et al. 1985; Rodríguez et al. 2000). The data were calibrated following the standard procedures in the AIPS (Astronomical Image Processing System) software package of NRAO and then concatenated in a single file.

The second image was made with the Karl G. Jansky Very Large Array of NRAO in the C (4.4 to 6.4 GHz) and X (7.9 to 9.9 GHz) bands during 2012 May 26 (2012.40), under project 12A-240. The central frequency of the image was 7.15 GHz. At that time the array was in its B configuration. The phase center was at $\alpha(2000) = 05^h 36^m 22^s.00$; $\delta(2000) = -06^\circ 46' 07''.0$. The absolute amplitude calibrator was 0137+331 and the phase calibrator was J0541-0541. The digital correlator of the JVLA was configured at each band in 16 spectral windows of 128 MHz width, each subdivided in 64 channels of 2 MHz. The total bandwidth of the observations was about 2.048 GHz in a full-polarization mode. The data were analyzed in the standard manner using the CASA (Common Astronomy Software Applications) package of NRAO.

Both images were restored with the synthesized beam of the 2012.40 observations, $1''.47 \times 0''.94$; $PA = -24^\circ$, and are shown in Figure 1.

⁴The National Radio Astronomy Observatory is a facility of the National Science Foundation operated under cooperative agreement by Associated Universities, Inc.

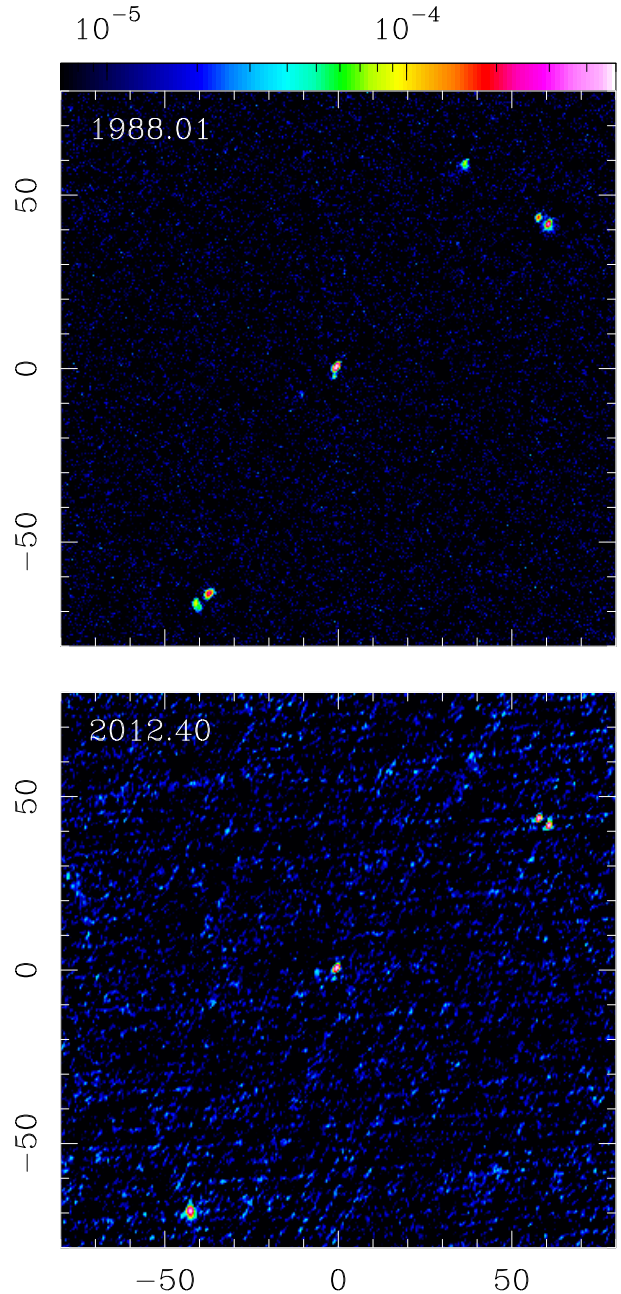


Fig. 1. VLA radio continuum maps at 4.86 GHz of the HH 1-2 region obtained in 1988.01 (top) and at 7.15 GHz in 2012.40 (bottom). The axes are labeled with offsets (in arcsec) from the position of the VLA 1 outflow source (N is up and E to the left). HH 1 is the emission at the approximate position $(40, 60)''$, and HH 2 at $(-40, -65)''$. The emission of the region around the Cohen-Schwartz star is seen in the 1988 map at $(20, 30)''$. The maps are shown with the logarithmic color scale given (in mJy per beam) by the top bar. The color figure can be viewed online.

2.2. Hubble Space Telescope

We compare the VLA maps with the four epochs of HH 1/2 H α images available in the HST archive:

- 1994.61: 3000s exposure (Hester et al. 1998),
- 1997.58: 2000s exposure (Bally et al. 2002),
- 2007.63: 2000s exposure (Hartigan et al. 2011),
- 2014.63: 2686s exposure (Raga et al. 2015a).

The calibration of these images and the errors in the determined line fluxes are described in detail by Raga et al. (2016a).

These images have been placed in approximately the same coordinate system as the VLA maps by centering the positions of the emission of the near environment of the Cohen-Schwartz star (visible in the H α images and in the 1988.01 VLA map). This results in a $\approx 0''.2$ shift of the H α images with respect to the positions derived from an astrometric calibration obtained using the positions of the C-S star and “star number 4” of Strom et al. (1985).

Figures 2 and 3 show the H α emission regions around HH 1 and 2 (respectively) in the four available epochs. In these figures we show the shifting, circular diaphragms (of $3''$ radius for HH 1 and $6''$ radius for HH 2) that we have used to compute H α fluxes to compare with the free-free radio continuum fluxes obtained from the VLA maps.

3. THE FREE-FREE AND H α EMISSION

Figures 4 and 5 show a comparison between the free-free continuum and the H α emission of HH 1 and 2 (respectively). These figures show superpositions of the 1988 VLA map and the 1997 H α image (top frames) and of the 2012 VLA map and the 2014 H α image (bottom frames of Figures 4 and 5).

For HH 1, we see that both the H α and free-free emission show a clear drop between the first and second epochs (Figure 4). We also see shifts in the positions of the radio continuum and H α emission peaks. These shifts are at least partly due to the proper motion of HH 1 (of $\approx 300 \text{ km s}^{-1}$, see Raga et al. 2016b), which corresponds to $\approx 0''.3$ in the 2012-2014 time span (bottom frame) and $\approx 1''.4$ in the 1988-1997 time difference (top frame of Figure 4) between the VLA and the H α maps.

For HH 2, we see that the 1988 VLA map shows two separate condensations (H to the SE and A to the NW, top frame of Figure 5). By 2012, condensation A has basically disappeared, and condensation H has strengthened considerably (bottom frame). A

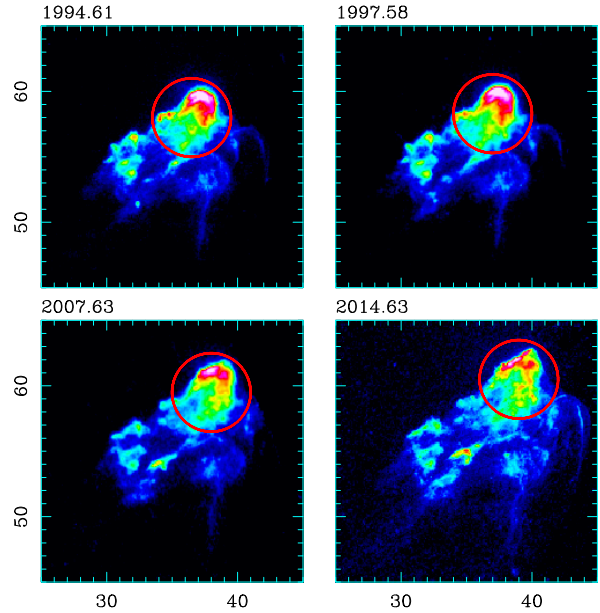


Fig. 2. H α images of HH 1 in the four available epochs of HST images. The axes are labeled as offsets (in arcsec) from the position of the VLA 1 outflow source. The circular diaphragms (of $3''$ radii) shown in the images have been used to compute H α fluxes. The images are displayed with a logarithmic color scale. The color figure can be viewed online.

similar effect is seen in the H α emission. In the comparison between the 2012 radio continuum and the 2014 H α emission we see a clear morphological difference, which probably cannot be fully attributed to the proper motion of HH 2 (which corresponds to a shift of only $\approx 0''.3$ to the SE between 2012 and 2014, see Raga et al. 2016c).

4. THE H α TO FREE-FREE CONTINUUM RATIOS

In Figure 6 we show the H α flux within the diaphragms shown in Figures 2 and 3 (for HH 1 and 2, respectively). This figure also shows the radio continuum flux (integrated over diaphragms of the same sizes as the ones used for H α) in the two available epochs.

It is clear that the H α and radio continuum fluxes both show an increasing trend of flux vs. time for HH 2, and a decreasing trend for HH 1. Within the errors, the observed trends (in the radio continuum and in H α) are similar for both HH 1 and 2.

In order to estimate the ratio between the H α flux and the free-free continuum, we use the 2014 H α and the 2012 continuum fluxes, because they are the pair of values closest in time. These two fluxes

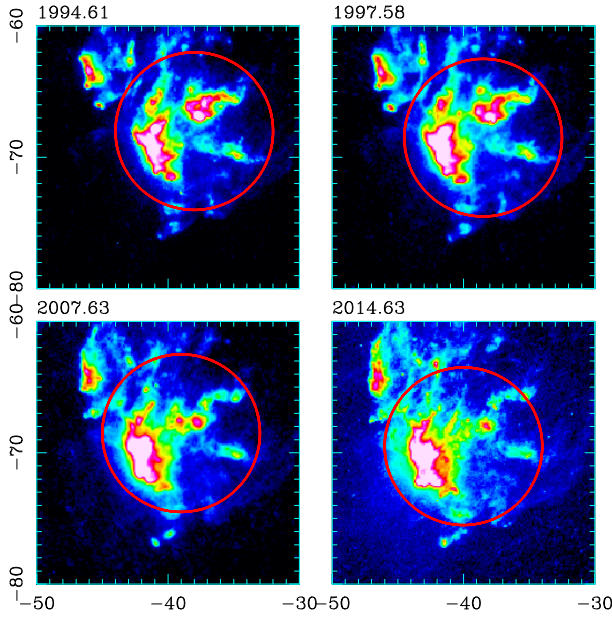


Fig. 3. $H\alpha$ images of HH 2 in the four available epochs of HST images. The circular diaphragms (of $6''$ radii) shown on the images have been used to compute $H\alpha$ fluxes. The images are displayed with a logarithmic color scale. The color figure can be viewed online.

TABLE 1

$H\alpha$ AND FREE-FREE FLUXES AND RATIOS

	HH 1	HH 2
F_{ff}^1	0.20 ± 0.02	1.53 ± 0.02
$F_{H\alpha}^2$	2.60 ± 0.16	29.6 ± 1.8
$F_{H\alpha}/F_{\text{ff}}^3$	1.30 ± 0.09	1.94 ± 0.14
$F_{H\alpha,0}/F_{\text{ff}}^{3,4}$	2.34 ± 0.16	3.50 ± 0.25

¹Free-free fluxes in mJy.

²Observed $H\alpha$ fluxes in $10^{-13} \text{ erg s}^{-1} \text{ cm}^{-2}$.

³Ratios in $10^{-12} \text{ erg s}^{-1} \text{ cm}^{-2} \text{ mJy}^{-1}$.

⁴Dereddened free-free/ $H\alpha$ ratio.

and their ratios are given in Table 1 (for HH 1 and 2). Using the 1997 $H\alpha$ and 1988 radio continuum fluxes (see Figure 6), one obtains similar line to continuum ratios.

These line-to-continuum ratios are most interesting. In order to compare them with theoretical predictions of this ratio, we should correct the observed values for interstellar extinction. As discussed by Raga et al. (2016a), for an $E(B - V) = 0.27$ and a standard Galactic extinction curve in order to obtain the dereddened $H\alpha$ flux, one has to multiply the observed flux by a factor of 1.80. The result-

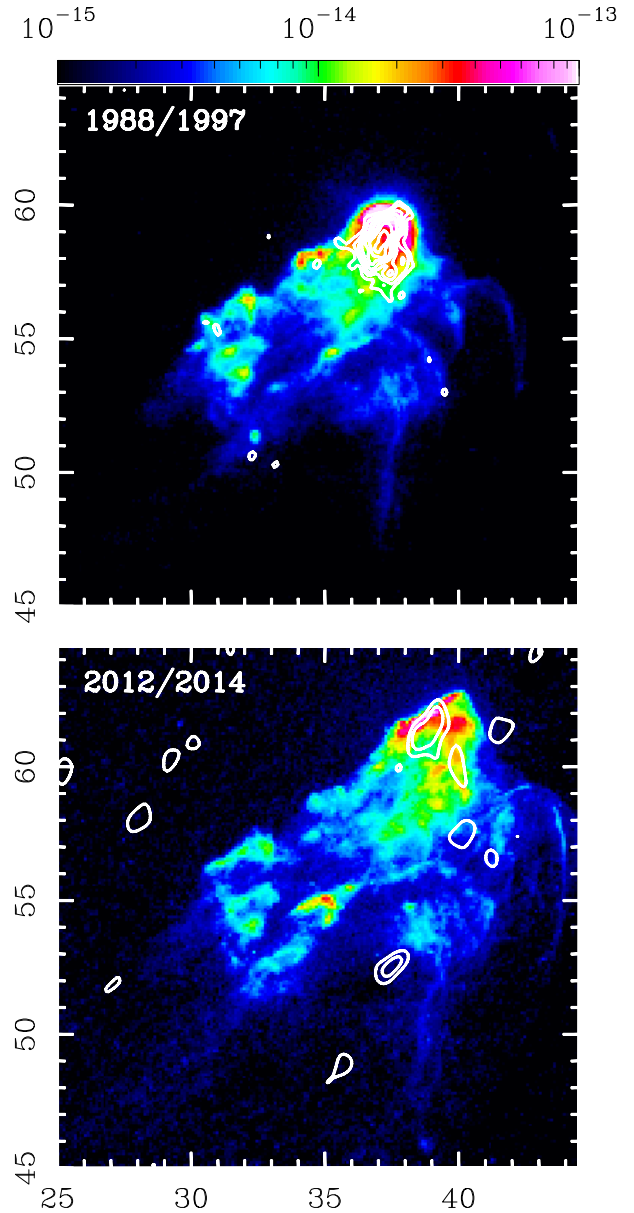


Fig. 4. Top: 1988 VLA map and 1997 $H\alpha$ image and bottom: 2012 VLA map and 2014 $H\alpha$ image of HH 1. The VLA maps are displayed with linear contours (the bottom contour corresponding to 25 and a linear step of $10 \mu\text{Jy}$ per beam). The $H\alpha$ maps are displayed with the logarithmic color scale given (in $\text{erg cm}^{-2} \text{ s}^{-1}$) by the top bar. The color figure can be viewed online.

ing, dereddened line to continuum ratios (calculated with the 2012 VLA map and the 2014 $H\alpha$ image) are given in Table 1.

We can compare the dereddened $F_{H\alpha,0}/F_{\text{ff}}$ values obtained for HH 1 and 2 with the prediction for this ratio obtained from equation (2) of Reynolds (1992).

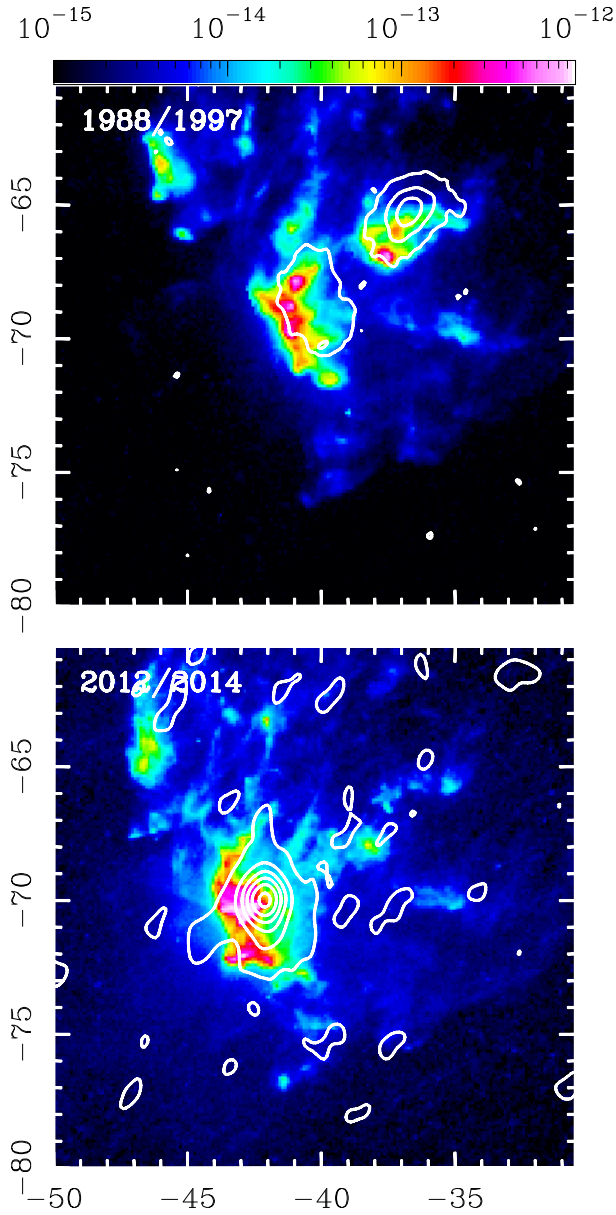


Fig. 5. Top: 1988 VLA map and 1997 H α image and bottom: 2012 VLA map and 2014 H α image of HH 2. The VLA maps are displayed with linear contours (the bottom contour corresponding to 25 and a linear step of 100 μ Jy per beam). The H α maps are displayed with the logarithmic color scale given (in $\text{erg cm}^{-2} \text{s}^{-1}$) by the top bar. The color figure can be viewed online.

The predicted temperature dependence for this ratio is shown in Figure 7. In this Figure, we also show horizontal lines corresponding to the dereddened ratios obtained for HH 1 (short dashes) and HH 2 (long dashes). It is clear that the observed ratios would

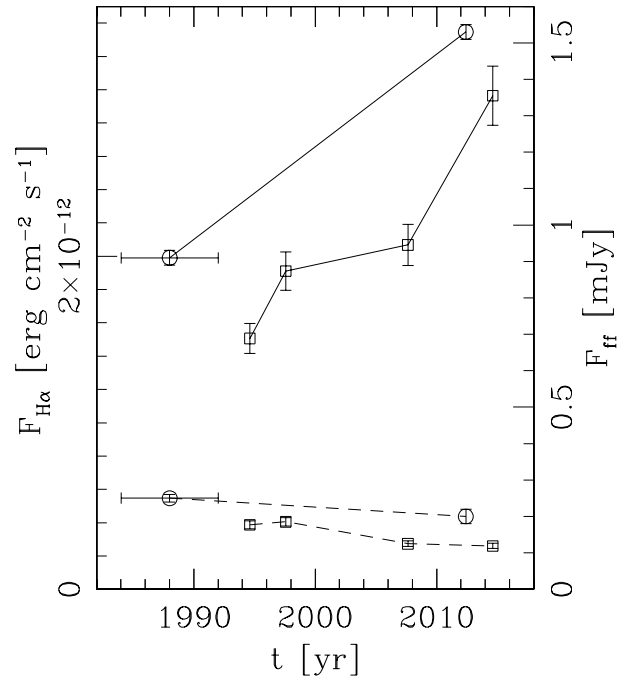


Fig. 6. H α fluxes (open squares) and radio continuum fluxes (open circles) as a function of time. The horizontal bars indicate the time interval over which the 1988 image was obtained. The HH 1 fluxes are joined by dashed lines, and the HH 2 fluxes are joined by solid lines. The scale of the H α fluxes is given on the left axis and the scale of the radio continuum fluxes is given on the right axis.

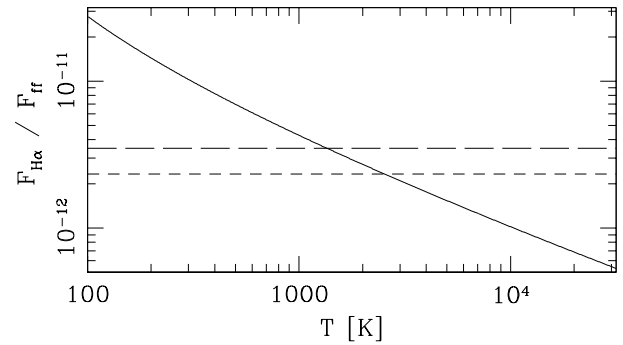


Fig. 7. The solid line shows the predicted ratio of the recombination H α flux (in $\text{erg cm}^{-2} \text{s}^{-1}$) to the 4.86 GHz free-free continuum (in mJy) as a function of temperature. The large dash and small dash lines show the values of the dereddened ratios found for HH 1 and 2 (respectively).

imply that the emission has a dominant contribution from regions with $T \approx 1000 \rightarrow 3000$ K.

5. COMPARISON WITH THE RADIO CONTINUUM AND $H\alpha$ EMISSION OF PNE

To determine observationally the expected $F_{H\alpha}/F_{\text{ff}}$ ratio for photoionized nebulae, we used the catalogs of Frew et al. (2013) and Parker et al. (2016) to select planetary nebulae with the following criteria:

- i) a determined 6-cm flux density with value ≥ 1 mJy,
- ii) a determined $H\alpha$ flux,
- iii) a determined logarithmic extinction at $H\beta$, c_β , from which the logarithmic extinction at $H\alpha$ can be obtained (Frew et al. 2013) as

$$c_\alpha = 0.70 \times c_\beta.$$

Planetary nebulae are the better objects for this determination since HII regions can suffer from very large extinction. We found a total of 211 planetary nebulae that comply with the above criteria. In Figure 8 we plot their extinction-corrected $H\alpha$ flux as a function of their 6-cm flux density. We fitted these data points with a linear function with slope 1. The least-squares fit gives

$$\log_{10} F_{H\alpha} = -(12.0 \pm 0.1) + \log_{10} F_{6\text{cm}},$$

where $F_{H\alpha}$ is given in $\text{erg cm}^{-2} \text{s}^{-1}$ and $F_{6\text{cm}}$ is given in mJy. This fit suggests (see Figure 7) that the H_α/H_{ff} ratio in planetary nebula can be explained on the average as coming from photoionized gas at a temperature of $\approx 10^4$ K.

In the same Figure we show the fluxes of HH1 and HH2, and it can be seen that their $F_{H\alpha}/F_{\text{ff}}$ ratios are a factor of ≈ 2 to 4 larger than the average value for planetary nebulae. These departures from the mean are, however, not very significant given the high dispersion of the planetary nebulae data. The mean and standard deviation of $\log_{10}(F_{H\alpha}/F_{6\text{cm}})$ for the planetary nebulae are -12.0 ± 0.3 and thus the HH objects are separated from the planetary nebulae mean only by 1-2 standard deviations (see Table 1).

We note that we have not taken into account two small effects. On one hand, the free-free emission can have a contribution from ionized helium. This could introduce an extra contribution of the order of 10% to the free-free emission from pure hydrogen. On the other hand, the planetary nebulae radio data were taken at 6-cm (5 GHz), while the points shown for HH1 and HH2 were taken at 7.15 GHz. Assuming that we are observing optically thin free-free, the flux density is expected to go as $\nu^{-0.1}$ and this will introduce an underestimate in the 6-cm flux density of the HH objects of about 4%.

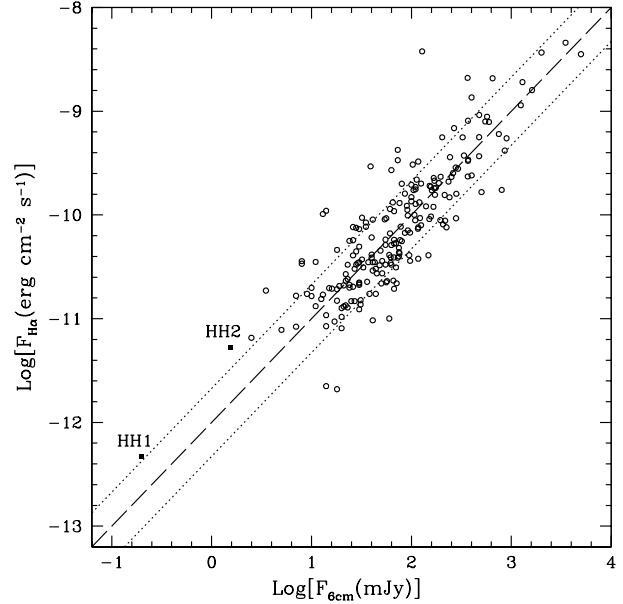


Fig. 8. $H\alpha$ flux versus 6-cm radio continuum flux for 211 planetary nebulae (empty circles). The dashed line shows the least squares fit to these points as discussed in the text. The dotted lines show the $\pm 1 \sigma$ ($\sigma = 0.33$) confidence interval. The positions of HH1 and HH2 are labeled and shown as filled squares.

The difference between the $F_{H\alpha}/F_{\text{ff}}$ ratios of PNe and of HH 1/2 is significant and a comparison with a larger sample of HH objects could be interesting. The straightforward explanation of this difference is that while all photoionized regions (in particular, PNe) have temperatures $\approx 10^4$ K (resulting from the balance of the photoionization heating and the strongly rising forbidden line cooling, see e.g. the book of Osterbrock 1974), the cooling region behind shock waves has emission at a range of decreasing temperatures. Particularly the $H\alpha$ emission (as well as the free-free emission) has a strong contribution from the dense, $T \approx 10^3$ K region towards the trailing edge of the recombination zone (this effect is discussed by Raga & Binette 1991, but is present in all plane-parallel shock models). Therefore, the fact that the $F_{H\alpha}/F_{\text{ff}}$ values of HH 1/2 imply a gas temperature of ≈ 2000 K (see Figure 7) is not surprising.

Another effect that could be affecting the HH 1/2 $F_{H\alpha}/F_{\text{ff}}$ ratio is that collisional excitation of $H\alpha$ appears to be taking place in part of the emitting regions of these objects (Raga et al. 2015b, c). However these regions have small angular extents, and do not contribute substantially to the angularly integrated emission of HH 1 and 2 (Raga et al. 2016a).

6. SUMMARY

We have presented a comparison of two VLA-JVLA radio continuum maps (epochs 1988 and 2012) with four HST H α images (1994, 1997, 2007 and 2014) of HH 1 and 2. We find that in both the radio continuum and H α images:

- HH 1 shows a trend of decreasing intensities with time,
- HH 2 shows a general trend of increasing intensities, with condensation H becoming much brighter and condensation A fading away.

The fact that both the radio and the optical emission show similar trends with time is quite conclusive evidence that the time-evolution of HH 1 and 2 is not due to a variation of the extinction (which could occur if the HH objects were moving into or away from regions with higher extinction). A change with time of the extinction towards the moving objects would affect the optical, but not the radio emission. This result agrees with Raga et al. (2016a) who reached a similar conclusion from an analysis of the time-dependence of the optical/UV emission line spectra of HH 1 and 2.

We find that the ratio $F_{H\alpha}/F_{\text{ff}}$ between the (angularly integrated) H α and free-free continuum fluxes of HH 1/2 agrees with the theoretical prediction obtained for a $T \approx 2000$ K emitting gas. This ratio is considerably higher than the one predicted for a 10^4 K temperature.

This effect shows up as a significant difference between the $F_{H\alpha}/F_{\text{ff}}$ values of HH 1/2 and the typical values obtained for a selection of PNe (with measured radio and H α fluxes), which on the average do have $\approx 10^4$ K temperatures, as expected for photoionized regions. This leads us to suggest that the value of $F_{H\alpha}/F_{\text{ff}}$ is an interesting diagnostic that can be used to discriminate between HH objects and photoionized regions. However, there appear to be a significant fraction of planetary nebulae as cool as the HH objects and this issue deserves further research.

We are thankful to R. Estalella for his valuable comments. This research has made use of the HASH PN database at `hashpn.space`. ARA acknowledges

support from the CONACYT grants 167611 and 167625 and the DGAPA-UNAM grants IA103315, IA103115, IG100516 and IN109715. LFR acknowledges the support from CONACYT, México and DGAPA, UNAM.

REFERENCES

- Bally, J., Heathcote, S., Reipurth, B., et al. 2002, *AJ*, 123, 2627
- Cohen, M. & Schwartz, R. D. 1979, *ApJ*, 233, L77
- Frew, D. J., Bojčić, I. S., & Parker, Q. A. 2013, *MNRAS*, 431, 2
- Haro, G. 1952, *ApJ*, 115, 572
- Hartigan, P., Foster, J. M., Wilde, B. H., et al. 2011, *ApJ*, 736, 29
- Herbig, G. H. 1951, *ApJ*, 113, 697
- . 1968, in *Non-Periodic Phenomena in Variable Stars*, ed. L. Detre (Dordrecht: Reidel), 75
- . 1973, *IBVS*, 832, 1
- Herbig, G. H. & Jones, B. F. 1981, *AJ*, 86, 1232
- Hester, J. J., Stapelfeldt, K. R., & Scowen, P. A. 1998, *AJ*, 116, 372
- Osterbrock, D. E. 1974, *Astrophysics of Gaseous Nebulae* (San Francisco: CA: Freeman)
- Parker, Q. A., Bojčić, I. S., & Frew, D. J. 2016, *JPhCS*, 728, 2008
- Pravdo, S. H., Rodríguez, L. F., Curiel, S., et al. 1985, *ApJ*, 293, L35
- Raga, A. C. & Binette, L. 1991, *RMxAA*, 22, 265
- Raga, A. C., Castellanos-Ramírez, A., Esquivel, A., Rodríguez-González, A., & Velázquez, P. F. 2015, *RMxAA*, 51, 231
- Raga, A. C., Reipurth, B., Castellanos-Ramírez, A., & Bally, J. 2016a, *RMxAA*, 52, 347
- Raga, A. C., Reipurth, B., Castellanos-Ramírez, A., Chiang, Hsin-Fang, & Bally, J. 2015a, *AJ*, 150, 105
- . 2015b, *ApJ*, 798, L1
- Raga, A. C., Reipurth, B., Esquivel, A., & Bally, J. 2016b, *AJ*, 151, 113
- Raga, A. C., Reipurth, B., Velázquez, P. F., Esquivel, A., & Bally, J. 2016c, *AJ*, 152, 186
- Rodríguez, L. F., Delgado-Arellano, V. G., & Gómez, Y. 2000, *AJ*, 119, 882
- Rodríguez, L. F., Ho, P. T. P., Torrelles, J. M., Curiel, S., & Cantó, J. 1990, *ApJ*, 352, 645
- Strom, S. E., Strom, K. M., Grasdalen, G. L., et al. 1985, *AJ*, 90, 2281

- C. Carrasco-González: Instituto de Radioastronomía y Astrofísica, Universidad Nacional Autónoma de México, A. P. 3-72 (Xangari), 58089 Morelia, Michoacán, México (c.carrasco@crya.unam.mx).
- A. C. Raga: Instituto de Ciencias Nucleares, Universidad Nacional Autónoma de México, Ap. 70-543, 04510 Cd. Mx., México (raga@nucleares.unam.mx).
- L. F. Rodríguez: Instituto de Radioastronomía y Astrofísica, Universidad Nacional Autónoma de México, A. P. 3-72 (Xangari), 58089 Morelia, Michoacán, México (l.rodriguez@crya.unam.mx).
- A. Rodríguez-Kamentzky: Instituto de Astronomía Teórica y Experimental, (IATE-UNC), X5000BGR Córdoba, Argentina (adrianark@gmail.com).